COBEM 2021 26th International Congress of Mechanical Engineering
November 22-26, 2021, Virtual Congress, Brazil

COB-2021-0368
ENERGY AND EXERGY ANALYSIS OF HYDROGEN PRODUCTION VIA HIGH-TEMPERATURE ELECTROLYSIS POWERED BY SOLAR AND WIND ENERGY

Diego Luis Izidoro
Engineering Academic Area, Instituto Federal de Educação, Ciência e Tecnologia de Minas Gerais (IFMG) - Campus Formiga, Padre Alberico Street, 440 - Formiga, MG, Brazil
diego.izidoro@ifmg.edu.br
Silvio de Oliveira Junior
Laboratory of Environmental and Thermal Engineering (LETE), Polytechnic School, Universidade de São Paulo (USP), Professor Mello Moraes Avenue, 2231 - São Paulo, SP, Brazil
soj@usp.br

Abstract. *Due to its high availability and production flexibility, hydrogen is seen as a promising alternative as an energy vector, besides being a raw material of great importance in chemical industries. However, almost all of the hydrogen used in the world nowadays is produced from fossil fuels. Therefore, it is essential that routes of hydrogen production from renewable energy sources must be developed and prioritized. In this way, this study evaluates a high-temperature electrolysis (HTE) process powered by solar and wind energy for clean hydrogen production. For that, a plant using solid oxide electrolysis cells (SOEC) is proposed. A 10 MW wind farm is considered to supply electricity, and a solar tower system provides thermal energy to the plant. Due to its high solar and wind resources, Guamaré, a coastal city located in northeastern Brazil, was selected as a case study. Energy and exergy analyses were performed. For a daily operation of eight hours, the average electricity generation was estimated at 122.38 MWh per day, and the solar energy needed for the heliostats was calculated at 44.50 MWh, which would be enough to produce 3.3 t/day of hydrogen. The electrolyzer achieved an exergy efficiency of 89.4%, and the average exergy efficiency of the plant was 31.7%. The solar receiver and the heat exchangers were the components with the lowest exergy efficiencies values. From this study, it is possible to carry out other analyses to improve and optimize the system and determine its economic viability for sustainable hydrogen production.*

Keywords: *exergy analysis, high-temperature electrolysis, hydrogen production, solar energy, wind energy.*

1. INTRODUCTION

The global energy demand has increased significantly and most of the energy is still obtained from fossil fuels, which are highly harmful to the environment. For this reason, the search for alternative energy sources has gained increasing importance in recent decades. In this context, hydrogen has a substantial potential to accelerate the process of scaling up clean and renewable energy.

Hydrogen as an energy vector/source has two significant advantages: low pollution, as its burning generates only water, and high calorific value. In addition to its use in refineries, it is used as a raw material in the chemical industries in the synthesis of ammonia and methanol, for example, in steel mills in the manufacture of steel and the food industries in the hydrogenation of oils (Abdin et al., 2020).

Hydrogen can be produced through different processes (thermochemical, electrochemical, and biological) and from various sources from both renewable technologies and fossil fuels. Hydrogen production from fossil fuels can be through steam reforming, partial oxidation, autothermal oxidation, and gasification. Generation of hydrogen from renewable sources can be through the gasification of biomass/biofuels and water splitting by solar energy or wind energy (Abdalla et al., 2018). However, less than 0.7% of current hydrogen production is from renewables, and its production is responsible for annual CO_2 emissions equivalent to those of Indonesia and the United Kingdom combined (IEA, 2019). Therefore, hydrogen production routes from renewable sources are developed and prioritized.

Solar/wind hydrogen production from water is a sustainable alternative to the traditional hydrogen production route using fossil fuels, and power-to-hydrogen is a promising solution for storing variable renewable energy to achieve a 100% renewable and sustainable hydrogen economy. Thus, the objective of this work is to propose a configuration of a hydrogen production plant based on high-temperature electrolysis (HTE) powered by wind and solar energy and perform energy and exergy analysis of this hybrid system to identify the points where the main energy losses and the highest exergy destruction rates are found. As a case study, wind and solar resources were considered for a typical meteorological year (TMY) for Guamaré, a city on the northeast coast of Brazil in the state of Rio Grande do Norte. Information about the analyzed technology, details about the methodology, and the main results of this study are presented below.

2. HIGH-TEMPERATURE ELECTROLYSIS

Water electrolysis is a well-known and established process. Basically, the principle of electrolysis is to convert water and electricity into gaseous hydrogen and oxygen, that is, the reverse of a hydrogen fuel cell. Nicholson and Carlisle first demonstrated this process in 1800. In the 1820s, Faraday clarified its principles, and in 1834 he introduced the word "electrolysis" (Laguna-Bercero, 2012). The use of electrolysis for hydrogen production has returned to the scientific spotlight since the oil crisis in the 1970s. Now, it is having another period of opportunity due to growing environmental concerns and the availability of renewable energy (Stempien et al., 2013).

There are two types of electrolyzers, depending on the operating temperature: Low-Temperature Electrolyzers (LTE) and High-Temperature Electrolyzers (HTE). While LTE operates at temperatures below 200°C, HTE operates at temperatures above 700°C. The main problem associated with LTEs is the high consumption of electricity. Although LTE is a mature technology, HTE has greater potential as water electrolysis becomes more endothermic with increasing temperature (O'Brien, 2012). HTE operates at reduced electrical potentials, and it results in a decrease in reaction overpotential and ohmic losses (Lin and Haussener, 2017).

The global reaction of water electrolysis can be represented by Eq. (1):

$$H_2O \rightarrow H_2 + 1/2\, O_2 \tag{1}$$

The minimum theoretical electrical energy ($\dot{W}_{min}$) required for the electrolysis process (reversible process) is given by Eq. (2), where ΔG is the variation of Gibbs free energy, ΔH is the change in enthalpy, T is the temperature, and ΔS is the variation of entropy:

$$\dot{W}_{min} = \Delta G = \Delta H - T\Delta S \tag{2}$$

The thermodynamic properties in Eq. (2) appear in Fig. 1a as a function of temperature for the H_2-H_2O system from 0°C to 1000°C at standard pressure. This figure is often cited as a motivation for high-temperature electrolysis versus low-temperature electrolysis, as the variation in the Gibbs free energy of the reaction (ΔG) decreases with increasing temperature, while the temperature product by changing entropy (TΔS) increases. Therefore, for reversible operation, the demand for electrical energy decreases with temperature, and a larger fraction of the total energy required for electrolysis (ΔH) can be supplied in the form of heat. This results in higher efficiencies for the process (O'Brien, 2012).

The technology used for high-temperature electrolysis is the solid oxide electrolyzer cell (SOEC). A simple scheme of a SOEC is illustrated in Fig. 1b. It consists of two porous electrodes (anode and cathode) and a dense ceramic electrolyte capable of conducting oxide ions (O^{2-}). The most common electrolytic material used is a dense ionic conductor of ZrO_2 doped with 8% of Y_2O_3 (YSZ) (Laguna-Bercero, 2012).

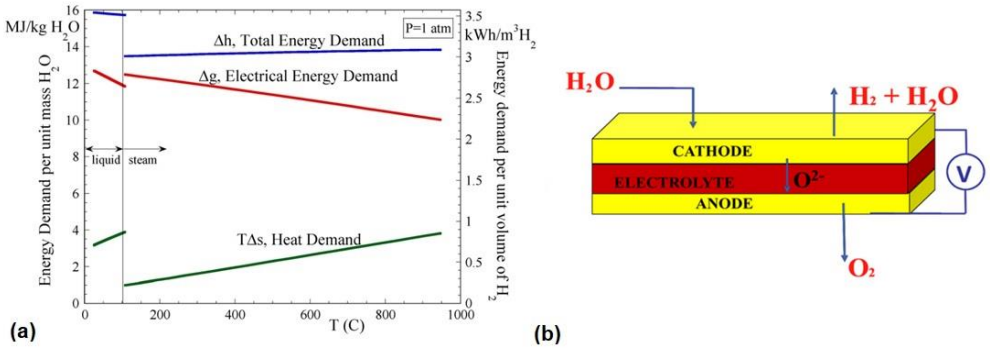

Figure 1. Water Electrolysis details: (a) Energy demand for the process (O'Brien, 2012); (b) Scheme of a SOEC (Laguna-Bercero, 2012).

SOECs have great flexibility for different applications. They can be used for direct electrochemical conversion of steam (H_2O), carbon dioxide (CO_2), or both into hydrogen (H_2) or syngas (H_2+CO), respectively. They also can be thermally integrated with a range of chemical syntheses, enabling the recycling of captured CO_2 and H_2O into synthetic natural gas or gasoline, methanol, or ammonia. When operated in reverse, a SOEC functions as a solid oxide fuel cell (SOFC). The most common ceramic SOECs typically work at 600° to 850°C. This technology has undergone formidable development and improvements over the past years in performance and durability and is approaching maturity. Furthermore, SOEC is based on scalable production methods and abundant raw materials. Therefore, due to these advantages, SOECs have a great potential to contribute to the integration of renewables in the energy matrix (Hauch et al., 2020).

3. METHODOLOGY

3.1 Proposed system

The proposed system for hydrogen production by high-temperature electrolysis is shown in Fig. 2. In this arrangement, a wind farm (WF) formed by five wind turbines with a rated power of 2 MW each supplies the electrical energy for the units of solid oxides electrolysis cells (SOEC). A solar tower system provides the thermal energy required for the process. Solar radiation is collected by the heliostats in the solar field (SF) and reflected in the solar receiver (SR) to superheat steam at a temperature of 850°C. From the electrolyzer, two streams, one of a mixture of hydrogen (H_2) and steam and the other of oxygen (O_2), go to the recovery heat exchangers (HX-1 and HX-5, respectively) to promote preheating of the water used in the electrolysis. In HX-2, the H_2/H_2O mixture is cooled and after that, the steam, now condensed, is separated from hydrogen and goes back to the beginning of the process. Finally, hydrogen and oxygen undergo compression processes (H_2 in CP-1 and CP-2 and O_2 in CP-3 and CP-4) and cooling (H_2 in HX-3 and HX-4 and O_2 in HX-6, HX-7, and HX-8) and go to be stored at a pressure of 30 bars. The wind farm also provides the electrical energy for the operation of the compressors. Due to the intermittence of electricity production, a connection to the electrical grid was considered.

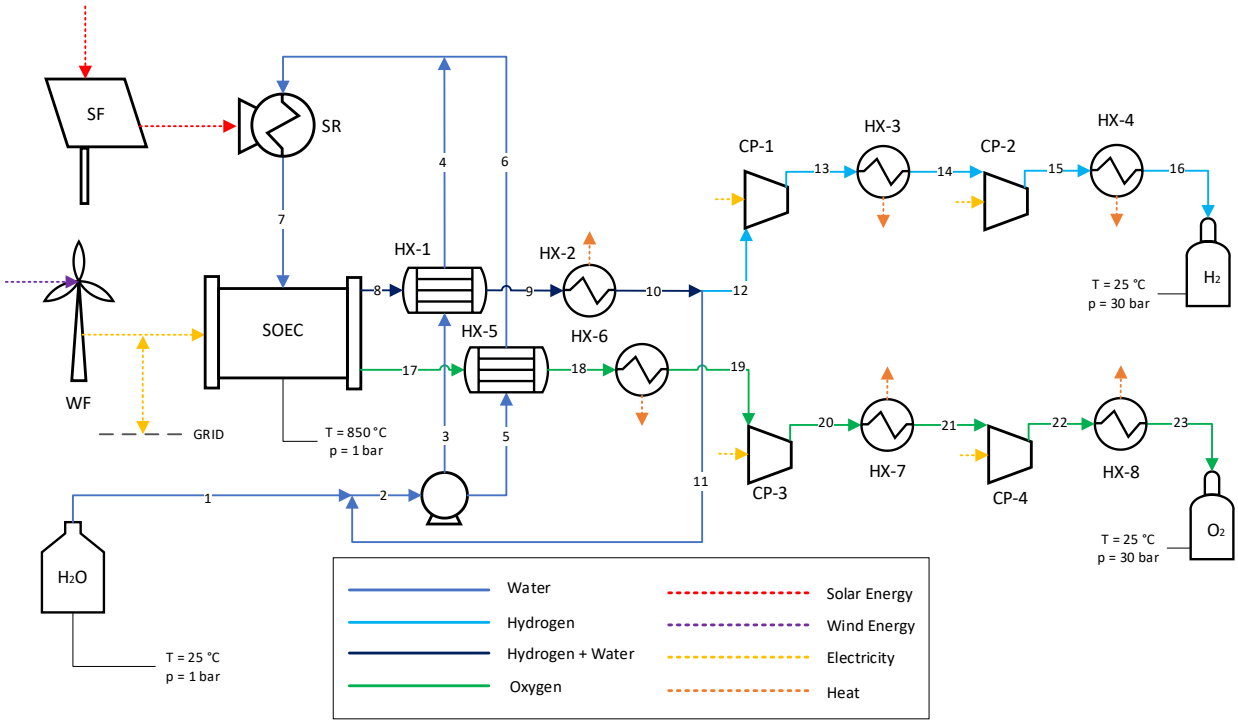

Figure 2. Proposed system

For the analysis of the proposed system, the following conditions were considered:

- The plant operates for eight hours a day, and hydrogen production takes place according to the supply of solar energy (Lin and Haussener, 2017). Thus, at each period of the day, a different number of electrolysis units is activated according to the level of solar radiation available;
- The efficiency conversion of AC-DC electricity from the wind farm/grid is 95%;
- The energy efficiency of the solar field (SF) is 60%, and the efficiency of the solar receiver (SR) is 85% (Xu et al., 2011);
- The electrolyzer operates at a thermoneutral voltage (V_{TN}) to minimize thermal stress (O'Brien, 2012). Thus, the process is adiabatic and isothermal, T = 850ºC and p = 1 bar;
- The molar steam conversion ratio (SC) is 75%, which means in practice that at the electrolyzer outlet, the molar fraction of H_2 is 0.75 (Petipas et al., 2013).
- The isentropic efficiency of each compressor is 80%;
- No heat transfers to the environment in the heat recovery exchangers HX-1 and HX-5. The minimum temperature difference (pinch point) is 10°C. The thermodynamic state of the water is the same at the outlet of these two exchangers;
- Pressure losses were not considered in the system, nor changes in kinetical and potential energy.

3.2 HTE Thermodynamics

The electrolyzer system model was developed according to O'Brien (2012) and Petipas et al. (2013). To accomplish electrolysis, the minimum necessary voltage for the reactions is the standard-state open-cell potential (V_0) given by Eq. (3), where ΔG is the Gibbs energy change, F is the Faraday constant (96486 C/mol), and j is the number of electrons transferred per molecule of hydrogen produced. In this case j = 2.

$$V_0 = \frac{\Delta G}{jF} \tag{3}$$

The standard-state open-cell potential (V_0) is applied to the case in which pure reactants and products are separated at standard atmosphere pressure (P_{std}). To account for the range of gas compositions and pressures that occur in real electrolyzers, the Nerst open cell potential (V_N), given by Eq. (4), must be considered, where R_u is the universal gas constant, y is the molar fractions of the steam and gases, T is the temperature and P is the pressure during the reaction.

$$V_N = V_0 - \frac{R_u T}{jF} ln\left[\left(\frac{y_{H2O}}{y_{H_2} y_{O2}^{1/2}}\right)\left(\frac{P}{P_{std}}\right)^{-1/2}\right] \tag{4}$$

The thermoneutral voltage (V_{TN}), in the function of the enthalpy of reaction (ΔH), is given by Eq. (5). The steam reduction reaction is endothermic, therefore the reaction heat flux ($q"_R$) is negative, but the ohmic heat flux ($q"_{OHM}$) is positive. The net heat flux is zero in the thermoneutral voltage because these heat fluxes cancel each other out. Their values can be calculated using Eq. (6), where i is the current density (A/m²).

$$V_{TN} = \frac{\Delta H}{jF} \tag{5}$$

$$q"_R = -q"_{OHM} = i(V_N - V_{TN}) \tag{6}$$

Finally, the electrical power ($\dot{W}_{TN}$) required for the electrolysis process considering thermoneutral voltage can be calculated using Eq. (7), where I is the current (A) in the electrolyzer and $\dot{m}_{H_2}$ is the hydrogen mass flow rate.

$$\dot{W}_{TN} = V_{TN} I = \dot{m}_{H_2} \Delta H \tag{7}$$

3.3 Solar and Wind Resources

This study was performed for Guamaré (Rio Grande do Norte), a coastal city located in northeastern Brazil. The location was chosen due to the high availability of solar and wind resources. In addition, Guamaré is located close to rivers and seaports, has more than 250 MW of wind farms in operation in its territory (Aneel, 2021), and is directly connected to the power transmission lines of the Brazilian electrical system (ONS, 2021). Furthermore, an oil refinery is also located in the city that produces diesel, gasoline, and aviation kerosene with a production capacity of 6000 m³/day (Petrobras, 2021). Therefore, it is a location that already has the necessary infrastructure to implement a hydrogen production plant.

Data for solar resource evaluation are taken from The National Solar Radiation Data Base (NRSDB) through System Advisor Model (SAM) software considering a typical meteorological year (TMY) (NREL, 2021). The hourly average direct normal irradiance (DNI) for Guamaré is presented in Fig. 3a, and the average daily DNI for each month is shown in Fig. 3b. For a year, the total direct irradiation is estimated at 2316 kWh/m² (an average of 6.34 kWh/m² per day).

For the wind resource evaluation, it was used the data from the atlas of Brazilian wind potential (CEPEL, 2017). The main wind parameters for Guamaré considering a height of 100 meters are presented in Tab. 1.

Table 1. Main wind parameters for Guamaré at 100 meters

Parameter	Unit	Value
Average wind speed ($\bar{v}$)	m/s	7.8
Scale factor (c)	-	8.5
Form factor (k)	m/s	4.8
Power density	W/m²	450
Average density of air (ρ)	kg/m³	1.18

Source: CEPEL (2017)

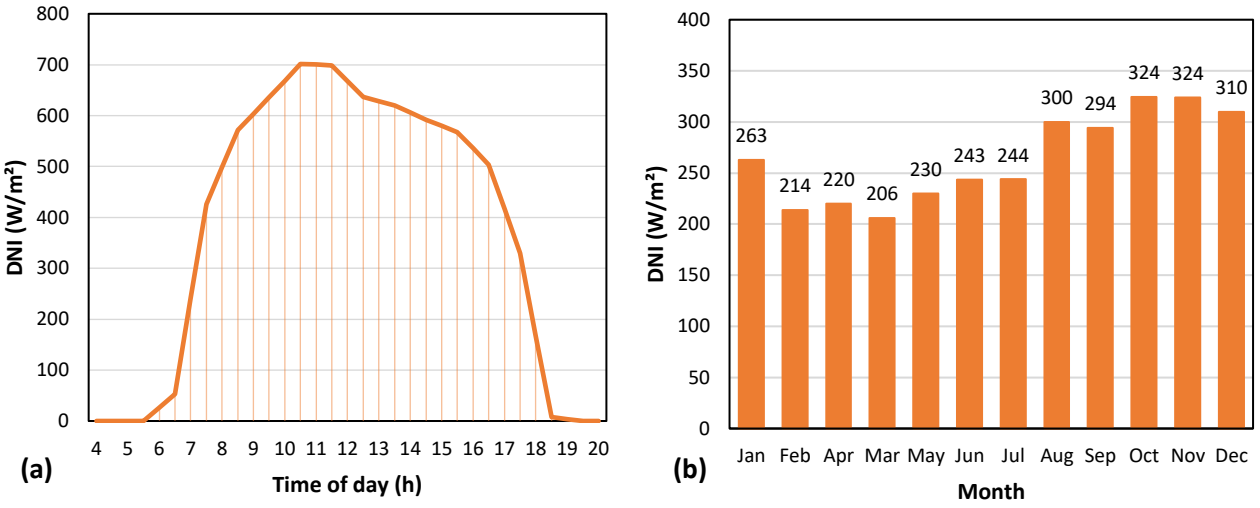

Figure 3. Solar irradiance for a typical year in Guamaré:
(a) Hourly average DNI ; (b) Daily average DNI for each month
(NREL, 2021).

The wind speed distribution can be represented by the Weibull density probability function, given by Eq. (8), where v is the wind speed, c is the scale factor, and k is the form factor (Pinto, 2018).

$$f(v) = \frac{k}{c}\left(\frac{v}{c}\right)^{k-1} e^{-(v/c)^k} \tag{8}$$

The Weibull function for Guamaré is shown in Figure 4a. By multiplying $f(v)$ by the number of total annual hours and integrating it into intervals of 1.0 m/s, it is obtained the histogram in Figure 5b, which shows the expected number of annual hours for each wind speed range. It is observed that speeds in the range between 6 and 10 m/s are prevalent.

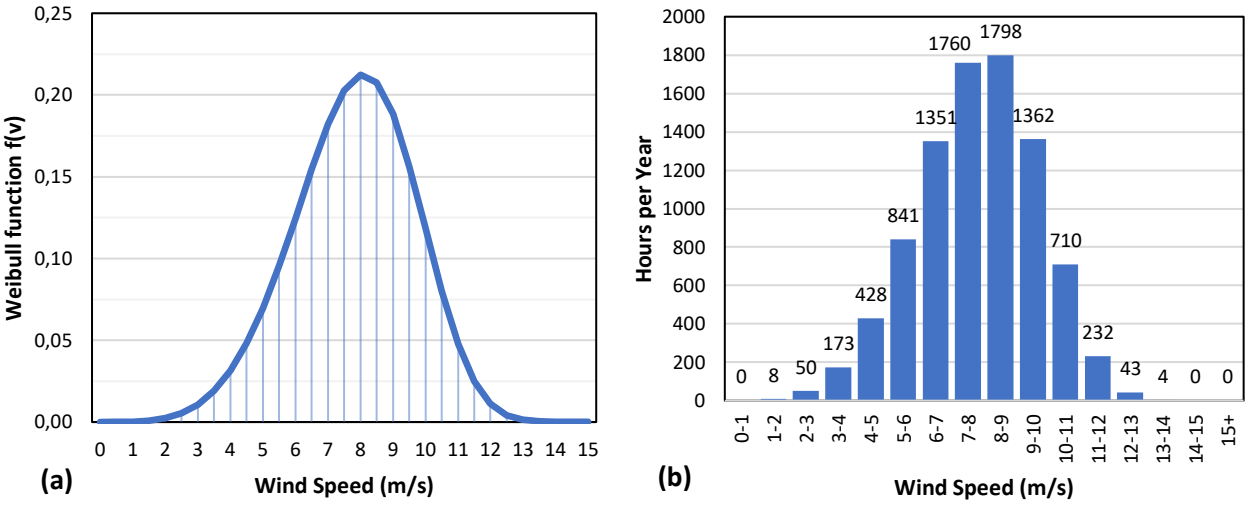

Figure 4. Wind resource for Guamaré: (a) Weibull distribution; (b) Annual hours for each wind speed range

For the analysis, the wind turbine Vestas V100-2MW was considered. This turbine has a hub height of 95 m, a rotor diameter of 100 m, and a swept area of 7854 m² (Vestas, 2021). For the wind farm in the SOEC model, it was considered five of these turbines, totalling 10 MW of rated power. The power curve of Vestas V100-2MW is presented in Figure 5. The average power generated ($\bar{W}_{WT}$) by each wind turbine can be calculated using Eq. (9), where $\dot{W}_{WT}(v)$ represents its power curve.

$$\bar{W}_{WT} = \int_0^{+\infty} \dot{W}_{WT}(v) \cdot f(v)\, dv \tag{9}$$

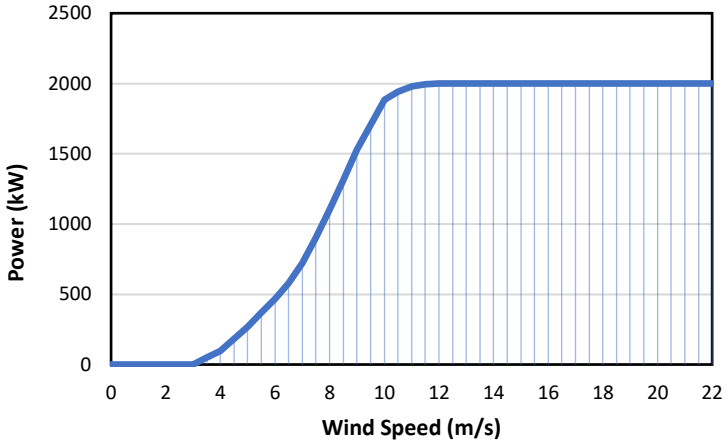

Figure 5. Wind turbine power curve (Vestas, 2021)

3.4 Energy and Exergy Analysis

The efficiency of electrolysis (η_{SOEC}) can be defined analogously to the definition for fuel cells in terms of the enthalpy of reaction according to Eq. (10), and the solar/wind-to-hydrogen conversion efficiency can be calculated in terms of the higher heating value of hydrogen (HHV) with Eq. (11):

$$\eta_{SOEC} = \frac{\dot{m}_{H_2} \Delta H}{\dot{W}} \tag{10}$$

$$\eta_{solar/wind\_H_2} = \frac{\dot{m}_{H_2} HHV_{H_2}}{\dot{W}_{WF,in} + \dot{Q}_{SF,in}} \tag{11}$$

The wind turbine exergy ($\dot{B}_{WF,in}$) is expressed by Eq. (12), where ρ is the air density, A is the turbine swept area, and v is the wind speed (Christopher and Dimitrios, 2012). For the exergy analysis of solar field (SF), the relation between energy and exergy fluxes in Eq. (13) was considered (Szargut. 2005), where T is the solar surface temperature (5778 K), and T_0 is the ambient temperature (298 K). For these values, the relationship between energy and exergy fluxes is 0.9312.

$$\dot{B}_{WF,in} = \frac{1}{2}\rho A v^3 \tag{12}$$

$$\frac{\dot{B}_{SF,in}}{\dot{E}_{SF,in}} = 1 - \frac{4}{3}\frac{T_o}{T} + \frac{1}{3}\left(\frac{T_0}{T}\right)^4 \tag{13}$$

The exergy efficiencies for the solar field (SF), solar receiver (SR), wind farm (WF), electrolyzer (SOEC), and heat exchangers HX-1 e HX-5 were defined as the ratio between input and output exergy. For the compressors, the exergy efficiencies were calculated as the ratio between the exergy change and the power supplied.

The total exergy efficiency of the plant was calculated as a function of the total fluids exergy rates and the solar radiation exergy rates with Eq. (14):

$$\eta_{ex\_total} = \frac{\dot{B}_{H_2.16} + \dot{B}_{O_2.23}}{\dot{B}_{WF,in} + \dot{B}_{SF,in} + \dot{B}_{water.1}} \tag{14}$$

4. RESULTS AND DISCUSSION

For the considered wind farm, the values of wind exergy and electricity generated in the function of the wind speed are shown in Figure 6a. Exergy efficiency values are shown in Figure 6b. The maximum net power (9.5 MW) is only reached above 11.6 m/s. This only occurs about 1.17% of the time, which corresponds to approximately 102 hours per year. The average net power was calculated in 5.01 MW. The maximum exergy efficiency (45.5%) is obtained for 5.5 m/s. The average annual value is 40%.

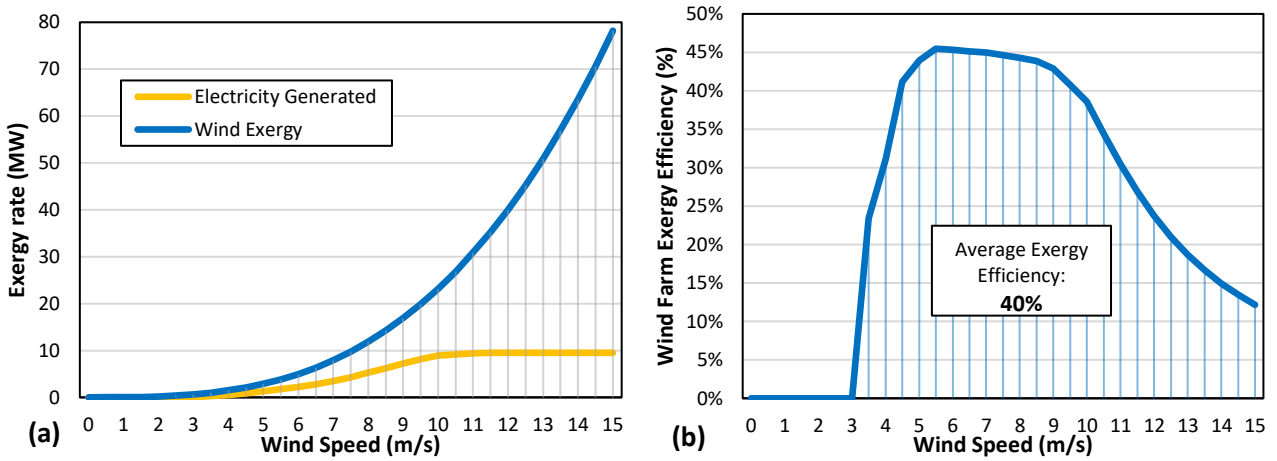

Figure 6. Wind farm results in function of the wind speed:
(a) Wind exergy and electricity generated; (b) Wind farm exergy efficiency

In Tab. 2 are presented the properties of water/steam, hydrogen, and oxygen at all points in the process. Values for physical exergy, chemical exergy, and total exergy flux (in kJ/kg) as well as exergy rates (in kW) are also presented considering the average value for hydrogen mass flow rate and adopted according to the standard model defined by Szargut (2005).

Table 2. Thermodynamic properties for the fluids in the proposed system(1)

Fluid	Point	$\dot{m}$ (kg/s)	T (°C)	P (bar)	h (kJ/kg)	s (kJ/kgK)	b_{ph} (kJ/kg)	B_{ph} (kW)	b_{ch} (kJ/kg)	B_{ch} (kW)	b_{total} (kJ/kg)	B_{total} (kW)
H_2O	1	1.024	25.0	1.01	104.92	0.37	0.00	0.00	0.27	0.28	0.27	0.28
	2	1.365	26.2	1.01	110.14	0.38	0.01	0.01	0.27	0.37	0.28	0.39
	3	1.002	26.2	1.01	110.14	0.38	0.01	0.01	0.27	0.27	0.28	0.28
	4		100.0	1.01	2200.95	6.08	392.01	392.75	477.07	477.97	869.08	870.73
	5	0.363	26.2	1.01	110.14	0.38	0.01	0.00	0.27	0.10	0.28	0.10
	6		100.0	1.01	2200.95	6.08	392.01	142.30	477.07	173.18	869.08	315.49
	7	1.365	850.0	1.01	4278.24	9.67	1399.82	1910.63	477.07	651.16	1876.89	2561.79
	11	0.341	30.0	1.01	125.82	0.44	0.17	0.06	0.27	0.09	0.45	0.15
H_2O+ H_2	8	0.456	850.0	1.01	7238.81	26.31	2410.75	1098.55	29797.02	13578.15	32207.77	14676.70
	9		100.0	1.01	2641.87	18.07	269.53	122.82	29440.07	13415.49	29709.61	13538.31
	10		30.0	1.01	1100.56	13.80	0.36	0.16	29440.07	13415.49	29440.43	13415.66
H_2	11	0.115	100.0	1.01	5011.32	56.61	116.74	13.37	117113.10	13415.40	117229.84	13428.77
	12		30.0	1.01	4003.38	53.61	0.59	0.07	117114.10	13415.51	117114.69	13415.58
	13		263.2	5.44	7380.67	54.93	2985.08	341.94	117113.10	13415.40	120098.18	13757.34
	14		30.0	5.44	4005.35	46.68	2070.76	237.21	117113.10	13415.40	119183.86	13652.61
	15		268.0	30.00	7469.24	48.02	5135.08	588.23	117113.10	13415.40	122248.18	14003.63
	16		25.0	30.00	3944.55	39.37	4187.30	479.66	117113.10	13415.40	121300.40	13895.06
O_2	17	0.909	850.0	1.01	1116.14	7.74	448.80	408.06	123.33	112.13	572.12	520.19
	18		36.2	1.01	281.36	6.44	0.19	0.17	123.33	112.13	123.52	112.31
	19		30.0	1.01	275.61	6.42	0.04	0.03	123.33	112.13	123.37	112.17
	20		253.2	5.44	486.83	6.51	186.30	169.38	123.33	112.13	309.62	281.52
	21		30.0	5.44	274.55	5.98	130.03	118.23	123.33	112.13	253.36	230.36
	22		258.1	30.00	490.20	6.07	320.43	291.34	123.33	112.13	443.75	403.47
	23		25.0	30.00	263.88	5.51	261.1	237.37	123.33	112.13	384.40	349.51

(1)Properties obtained using CoolProp (Bell et al. 2014) and chemical exergy values from Szargut (2005).

The hydrogen production for the proposed plant is illustrated in Fig. 7. The average daily production was estimated at 3.3 tons of H_2. Then, the output of O_2 would be 26.1 t/day and water consumption, 29.4 m³/day. The months with the highest production are October and November due to the higher availability of direct irradiation in these periods.

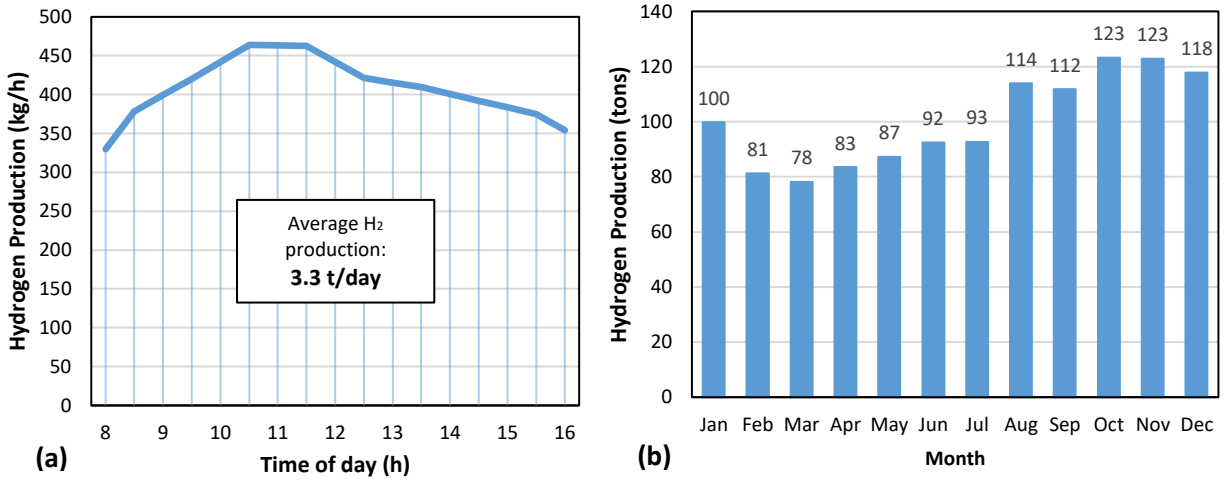

Figure 7. Hydrogen production for the proposed system:
(a) Average hourly production; (b) Average production per month

The results for the energy and exergy analysis for the wind farm, solar field, and solar receiver are summarized in Tab. 3. The irreversibilities in wind turbines are related to the interaction of the air and the blades and the mechanical and electrical conversion efficiencies. For the solar field, there are optical losses (attenuation, blocking, or shadowing) and losses related to heat convection and conduction. For the solar receiver, the low exergy efficiency is explained by the temperature difference in the steam and losses related to convection, conduction, and reflection, representing the largest portion of process losses (Petela, 2010). Because of this, the exergy change in the steam in the SR represents only 26.6% of the total solar exergy received in the solar field.

Table 3. Energy and exergy analysis: Solar/Wind subsystem

Components	Energy Analysis				Exergy Analysis			
	Received (MWh/day)	Delivered (MWh/day)	Loss (MWh/day)	Energy Efficiency (%)	Received (MWh/day)	Delivered (MWh/day)	Losses (MWh/day)	Exergy Efficiency (%)
Wind Farm (WF)	306.17	122.38	183.79	40.0	306.17	122.38	183.79	40.0
Solar Field (SF)	44.50	26.70	17.80	60.0	41.43	24.83	16.60	60.0
Solar Receiver (SR)	26.70	22.69	4.01	85.0	24.83	11.01	13.82	44.3 [(2)]

[(2)]Only physical exergy of the steam was considered for the calculation for the solar receiver.

In Tab. 4 are presented the results for the electrolyzer, heat exchangers, and compressors. In the electrolyzer, losses are associated with overvoltage at the anode and cathode and due to the ohmic resistance of the cells (Obrien, 2008). The thermoneutral voltage (V_{TN}) is equal to 1.288 V, the ohmic heat flux ($q"_{OHM}$) is 0.163 W/cm², and the average power consumed ($\dot{W}_{TN}$) was calculated at 14.13 MW, which corresponds to 92.3% of the electricity demand of the plant. Finally, the exergy efficiency is 89.4%. This value can be increased if the operating voltage is reduced. However, this would imply a non-zero net heat flux, causing operational difficulties.

The heat exchangers HX-1 and HX-5 used to recover heat from the electrolyzer output streams achieved high values of exergy destruction and, therefore, low exergy efficiencies. This is due to the high mean temperature difference between the fluids, which can be improved through changes in the proposed arrangement in this study. Another possibility for improvement is to recovery the rejected heat in the hydrogen and oxygen cooling exchangers. If the 441 kW of exergy were used to generate electricity, they could supply at least one of the compressors.

Considering the whole plant and the values presented in Tab. 3 and 4, the calculated solar/wind-to-hydrogen conversion efficiency was 37.1%, and the overall exergy efficiency, 32.7%. The energy and exergy losses are detailed in the Sankey and Grassmann diagrams, respectively, in Fig. 8a and 8b.

Table 4. Energy and exergy analysis: Electrolyzer and Gases Storage Subsystem

Components	Energy Analysis			Exergy Analysis		
	Power (kW)	Rejected (kW)	Energy Efficiency (%)	Destroyed (kW)	External Losses (kW)	Exergy Efficiency[3] (%)
Electrolyzer (SOEC)	14125.66	0	100.0	1490.56	0	89.4
Heat Exchanger 1 (HX-1)	-	0	100	583.00	0	40.2
Heat Exchanger 2 (HX-2)	-	702.35	-	0	122.66	-
Compressor 1 (CP-1)	386.87	0	100	44.9	0	88.4
Heat Exchanger 3 (HX-3)	-	386.65	-	0	104.74	-
Compressor 2 (CP-2)	396.79	0	100	45.77	0	88.5
Heat Exchanger 4 (HX-4)	-	403.76	-	0	108.57	-
Heat Exchanger 5 (HX-5)	-	0	100	265.57	0	34.9
Heat Exchanger 6 (HX-6)	-	5.23	-	0	0.14	-
Compressor 3 (CP-3)	192.05	0	100	22.70	0	88.2
Heat Exchanger 7 (HX-7)	-	193.01	-	0	51.15	-
Compressor 4 (CP-4)	196.07	0	100	22.96	0	88.3
Heat Exchanger 8 (HX-8)	-	205.77	-	0	53.96	-
Total	15297.44	1896.77	87.6	2475.46	441.22	80.9

[3]Only physical exergy was considered for the calculation of the heat exchangers.

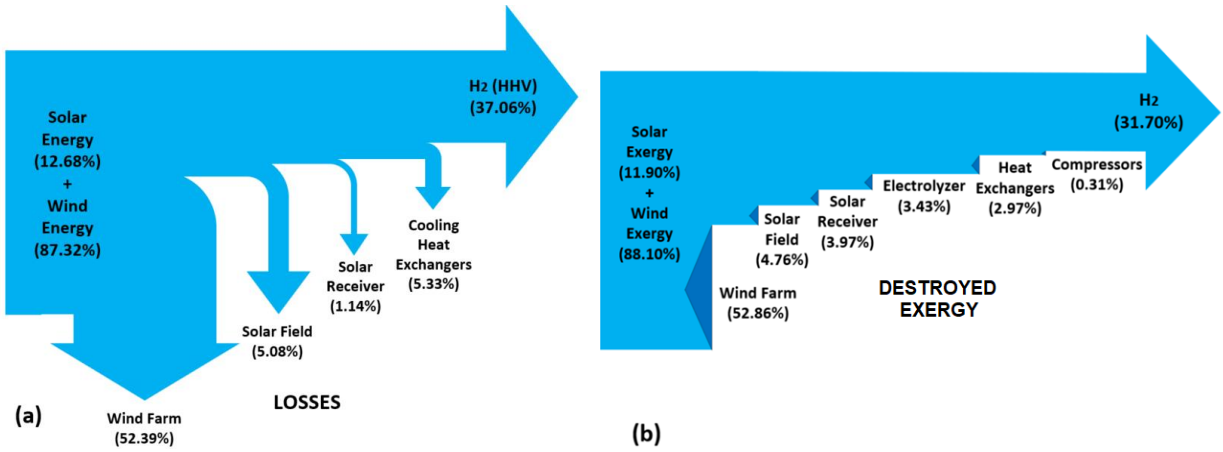

Figure 8. Energy and Exergy Diagrams: (a) Sankey; (b) Grassmann

5. CONCLUSIONS

In this paper, energy and exergy analysis of a high-temperature electrolysis process (HTE) was performed for solid oxide electrolysis cells (SOEC). The study was carried out for a proposed plant in Guamaré, a coastal city located in northeastern Brazil. In this plant, the thermal demand is supplied by solar energy from a solar tower system and the electrical demand by a wind farm.

For a daily operation of eight hours supplied by a 10 MW wind farm connected to the electrical grid, the thermal energy needed for the solar collectors was estimated at 44.50 MWh/day, which would be enough for an average daily production of 3.3 tons of hydrogen. The solar/wind-to-hydrogen conversion efficiency was 37.1%, and the overall exergy efficiency was 31.7%. The solar receiver (SR) and the heat exchangers presented the highest rates of destroyed exergy proportionally. Therefore, the plant's arrangement, especially these components, can be modified and optimized to increase their exergy efficiencies. In addition, other possibilities can be considered, such as energy storage for 24-hour operation, waste heat recovery in gas cooling heat exchangers, and operation of the electrolyzer in different thermodynamic conditions.

Regardless of the efficiency achieved, the process proves feasible from a technical and environmental point of view. An exergoeconomic analysis is also essential to assess the costs involved. Furthermore, the technological options considered in the proposed system are still in the process of research and development, and, therefore, they represent promising alternatives for the future for hydrogen production from renewable energy.

6. ACKNOWLEDGEMENTS

The first author acknowledges Instituto Federal de Educação, Ciência e Tecnologia de Minas Gerais (IFMG) - Campus Formiga for its financial support during the development of this study. The second author acknowledges CNPq (Brazilian National Council for Scientific and Technological Development) for the grant 306484/2020-0.

7. REFERENCES

Abdalla, Abdalla M., Shahzad Hossain, Ozzan B. Nisfindy, Atia T. Azad, Mohamed Dawood, and Abul K. Azad. 2018. “Hydrogen Production, Storage, Transportation and Key Challenges with Applications: A Review.” Energy Conversion and Management 165 (January): 602–27. https://doi.org/10.1016/j.enconman.2018.03.088.

Abdin, Zainul, Ali Zafaranloo, Ahmad Rafiee, Walter Mérida, Wojciech Lipiński, and Kaveh R. Khalilpour. 2020. “Hydrogen as an Energy Vector.” Renewable and Sustainable Energy Reviews 120 (November 2019). https://doi.org/10.1016/j.rser.2019.109620.

Annel. Agência Nacional de Energia Elétrica. 2021. “Sistema de Informações de Geração. https://www.aneel.gov.br/siga

ONS. Operador Nacional do Sistema Elétrico. 2021. Mapa Dinâmico do Sistema Elétrico Nacional (SIN). https://www.ons.org.br/paginas/sobre-o-sin/mapas.

Bell, Ian H, Jorrit Wronski, Sylvain Quoilin, and Vincent Lemort. 2014. “Pure and Pseudo-Pure Fluid Thermophysical Property Evaluation and the Open-Source Thermophysical Property Library CoolProp.”

CEPEL. Centro de Pesquisas de Energia Elétrica. 2017. Atlas do Potencial Eólico Brasileiro: Simulações 2013. Rio de Janeiro. 52 p.

Christopher, Koroneos, and Rovas Dimitrios. 2012. “A Review on Exergy Comparison of Hydrogen Production Methods from Renewable Energy Sources.” Energy and Environmental Science 5 (5): 6640–51. https://doi.org/10.1039/c2ee01098d.

Hauch, A., R. Küngas, P. Blennow, A. B. Hansen, J. B. Hansen, B. V. Mathiesen, and M. B. Mogensen. 2020. “Recent Advances in Solid Oxide Cell Technology for Electrolysis.” Science 370 (6513). https://doi.org/10.1126/science.aba6118.

IEA. 2019. The Future of Hydrogen: Seizing Today’s Opportunities. International Energy Agency. Japan: OECD. https://doi.org/10.1787/1e0514c4-en.

Laguna-Bercero, M. A. 2012. "Recent Advances in High-Temperature Electrolysis Using Solid Oxide Fuel Cells: A Review." Journal of Power Sources 203: 4–16. https://doi.org/10.1016/j.jpowsour.2011.12.019.

Lin, Meng, and Sophia Haussener. 2017. “Techno-Economic Modeling and Optimization of Solar-Driven High-Temperature Electrolysis Systems.” Solar Energy 155: 1389–1402. https://doi.org/10.1016/j.solener.2017.07.077.

NREL. National Renewable Energy Laboratory. 2021. NSRDB: National Solar Radiation Database. https://nsrdb.nrel.gov/

O'Brien, James E. 2012. "Thermodynamics and Transport Phenomena in High-Temperature Steam Electrolysis Cells." Journal of Heat Transfer 134 (3): 1–11. https://doi.org/10.1115/1.4005132.

Petela, R. 2010. “Engineering Thermodynamics of Thermal Radiation for Solar Power Utilization”. New York, McGraw Hill, 2010.

Petipas, Floriane, Annabelle Brisse, and Chakib Bouallou. 2013. "Model-Based Behaviour of a High-Temperature Electrolyser System Operated at Various Loads." Journal of Power Sources 239 (2013): 584–95. https://doi.org/10.1016/j.jpowsour.2013.03.027.

Petrobras. 2021. Nossas Atividades. Refinaria Potiguar Clara Camarão. https://petrobras.com.br/pt/nossas-atividades/principais-operacoes/refinarias/refinaria-potiguar-clara-camarao.htm.

Pinto, M. O. 2018. “Fundamentos de Energia Eólica”. Rio de Janeiro, LTC. 368 p.

Stempien, J., Q. Sun, and S. Chan. 2013. “Solid Oxide Electrolyzer Cell Modeling: A Review.” Journal of Power Technologies 93 (4): 216–46.

Szargut, J. 2005. “Exergy Method: Technical and Ecological Applications”. Southampton, UK: WIT Press.

Vestas. 2021. 2 MW platform. Technical specifications. https://www.vestas.com/en/products/2-mw-platform/

Xu, Chao, Zhifeng Wang, Xin Li, and Feihu Sun. 2011. “Energy and Exergy Analysis of Solar Power Tower Plants.” Applied Thermal Engineering 31 (17–18): 3904–13. https://doi.org/10.1016/j.applthermaleng.2011.07.038.

8. RESPONSIBILITY NOTICE

The authors are the only ones responsible for the printed material included in this paper.